Crystal structure of the calcium pump of sarcoplasmic reticulum at 2.6 Å resolution

Chikashi Toyoshima*†, Masayoshi Nakasako*†‡, Hiromi Nomura* & Haruo Ogawa*

** Institute of Molecular and Cellular Biosciences, The University of Tokyo, Bunkyo-ku, Tokyo 113-0032, Japan*
† The Harima Institute, The Institute of Physical and Chemical Research, Sayo-gun, Hyo-go 679-5143, Japan
‡ PRESTO, Japan Science and Technology Corporation, Kawaguchi 332-0012, Japan

Calcium ATPase is a member of the P-type ATPases that transport ions across the membrane against a concentration gradient. Here we have solved the crystal structure of the calcium ATPase of skeletal muscle sarcoplasmic reticulum (SERCA1a) at 2.6 Å resolution with two calcium ions bound in the transmembrane domain, which comprises ten α-helices. The two calcium ions are located side by side and are surrounded by four transmembrane helices, two of which are unwound for efficient coordination geometry. The cytoplasmic region consists of three well separated domains, with the phosphorylation site in the central catalytic domain and the adenosine-binding site on another domain. The phosphorylation domain has the same fold as haloacid dehalogenase. Comparison with a low-resolution electron density map of the enzyme in the absence of calcium and with biochemical data suggests that large domain movements take place during active transport.

The calcium pump of sarcoplasmic reticulum was first identified in the 'relaxing factor' of muscle contraction and gave rise to the calcium theory[1] that Ca^{2+} is a fundamental and ubiquitous factor in the regulation of intracellular processes. It is an integral membrane protein of relative molecular mass 110,000 (M_r 110K) and pumps Ca^{2+} released in muscle cells during contraction back into the sarcoplasmic reticulum using the chemical energy of ATP, thereby relaxing muscle cells. This pump is therefore an ATPase and a representative member of a group of enzymes called P-type ATPases; the name came from the fact that they are autophosphorylated (at Asp 351 with Ca^{2+}-ATPase) during the reaction cycle (for recent reviews, see refs 2–4). P-type ATPases are all ion pumps of crucial importance, for example Na^+K^+-ATPase and gastric H^+K^+-ATPase.

The amino-acid sequences of P-type ATPases have been known for some time, and secondary-structure prediction has proposed models with ten transmembrane helices (M1–M10)[5]. Extensive mutational studies have been carried out to identify the amino-acid residues that are critical for ion transport (for example, see ref. 3). Negatively charged residues on four putative transmembrane helices (M4–M6 and M8) have been postulated to form high-affinity binding sites[6]. The evolutionary connections with other enzyme families have been a long-standing issue, because P-type ATPases lack the P-loop commonly found in other ATPases and GTPases[7]. Nevertheless, marked homology with L-2-haloacid dehalogenase has been pointed out for the catalytic core of the cytoplasmic domain[8].

Direct structural information has so far been limited because the crystals that had been obtained were useful only for electron microscopy. Two types of crystal have been obtained for sarcoplasmic reticulum Ca^{2+}-ATPase: tubular crystals formed in the absence of Ca^{2+} and the presence of decavanadate[9]; and three-dimensional microcrystals formed in the presence of millimolar Ca^{2+} (refs 10, 11). From electron microscopy of these crystals, it is clear that the enzyme has a large cytoplasmic 'headpiece' connected to the transmembrane region by a short stalk segment[12,13], and that the headpiece appears to split on Ca^{2+} binding to the membrane domain[14].

Here we have improved the crystallization conditions and succeeded in growing crystals suitable for X-ray crystallography. We describe the structure of the sarcoplasmic reticulum calcium pump with two Ca^{2+} ions in the transmembrane binding sites at 2.6 Å resolution. The atomic model explains the 8 Å resolution map obtained from tubular crystals[13], suggesting that large concerted domain motions take place during active transport.

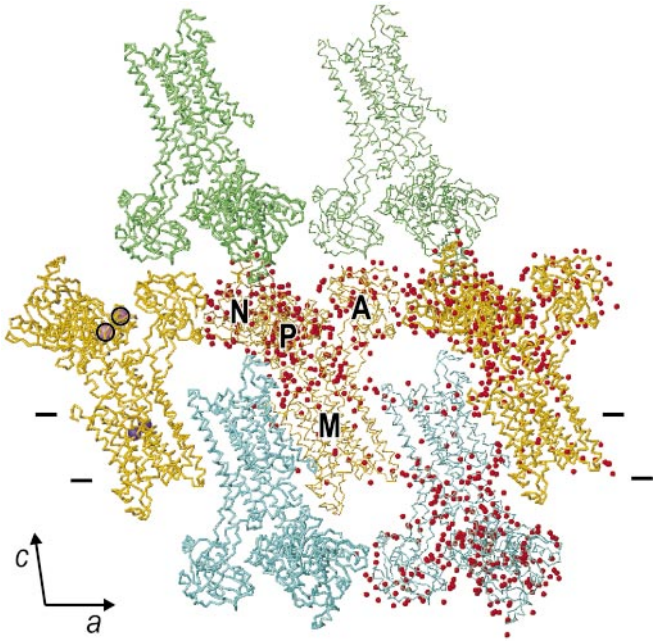

Figure 1 Crystal packing of Ca^{2+}-ATPase in the plate-like crystals. Cα traces with the *a* axis horizontal and the *b* axis normal to the plane of the paper. Thin lines represent the molecules offset by a half unit cell along the *b* axis owing to the crystal symmetry. Because the crystal is made of stacks of membranes, the lipid bilayers extend parallel to the *ab* plane (normal to the plane of the paper) but may well be distorted around the protein molecules. Horizontal bars show rough estimates of the positions of the membrane surface from the distribution of hydration water. Three cytoplasmic domains (A, N and P) are identified as in Fig. 2. Locations of two Ca^{2+} ions are indicated by spheres in violet in the transmembrane domain (M). Those of lanthanides (La^{3+} and Tb^{3+}) in derivative crystals (see Table 1) are marked by circles. No binding of lanthanides was detected in the transmembrane region. The distance between adjacent layers measures 145.7 Å.

Table 1 Summary of crystallographic analysis

Data set*	Concentration (mM)	Resolution (Å)	Completeness (%)	R_{merge}† (%)	Redundancy	I/σ	R_{iso}‡ (%)	No. of sites	Phasing power§
Native (eight crystals)		2.60	99.9	6.6 (25.9)#	27.2	29.3 (4.3)#			
PIP	1	3.20	98.0	6.1 (17.8)	3.4	23.7 (7.7)	10.2	1	0.40
$K_2Pt(NO_2)_4$	2	2.80	99.5	6.0 (21.5)	3.3	24.7 (6.7)	12.6	4	1.01
	0.4	3.10	99.8	6.9 (20.1)	3.8	25.6 (5.4)	8.7	4	1.02
$Pt(NH_3)_4(NO_3)_2$	1	3.10	99.8	6.8 (20.7)	3.6	16.8 (5.0)	5.9	2	0.45
$K_2Pt(CN)_6$	2	3.20	94.5	4.0 (13.3)	3.4	11.3 (5.6)	11.0	3	0.34
$Tb(NO_3)_3$	2	3.15	98.2	5.6 (18.1)	3.4	10.3 (4.2)	11.5	2	1.00
(soaked 90 h)	1	3.00	99.9	6.0 (18.2)	2.7	9.2 (4.7)	8.0	2	0.85
$La(NO_3)_3$	2	3.20	98.0	4.0 (13.0)	3.5	15.1 (6.0)	6.9	2	0.82
TNP-AMP	0.5	4.00	94.7	10.8 (18.1)	2.8	6.0 (4.1)	9.9		

Refinement statistics

Resolution range	No. of reflections	No. of protein atoms	No. of water molecules	No. of Ca^{2+} atoms	R_{cryst}‖ (%)	R_{free}¶ (%)	R.m.s. bond lengths (Å)	R.m.s. bond angle (°)
15–2.6 Å	48,373 (92.5%)	7,673	276	2	25.0	30.7	0.008	1.4

* Diffraction data were collected at SPring-8 (beamline BL41XU (λ = 0.800 Å) and BL44B2 (λ = 0.890 Å and 1.000 Å) for native crystals and BL44B2 (λ = 0.890 Å) for derivatives).
† $R_{merge} = \Sigma_{hkl}\Sigma_i |I_i(hkl) - \langle I(hkl)\rangle| / \Sigma_{hkl}\Sigma_i I_i(hkl)$.
‡ $R_{iso} = \Sigma_{hkl} ||F_{deriv}(hkl)| - |F_{native}(hkl)|| / \Sigma_{hkl} |F_{native}(hkl)|$.
§ Defined as the ratio of the r.m.s. value of the heavy atom structure factor amplitudes and the r.m.s. value of the lack-of-closure error.
‖ $R_{cryst} = \Sigma_{hkl} ||F_{obs}(hkl) - F_{calc}(hkl)|| / \Sigma_{hkl} F_{obs}(hkl)$.
¶ Same as R_{cryst}, but calculated with 10% of data set aside for refinement.
# The numbers in the parentheses refer to those in the last resolution shell (2.68–2.60 Å for the native data set).

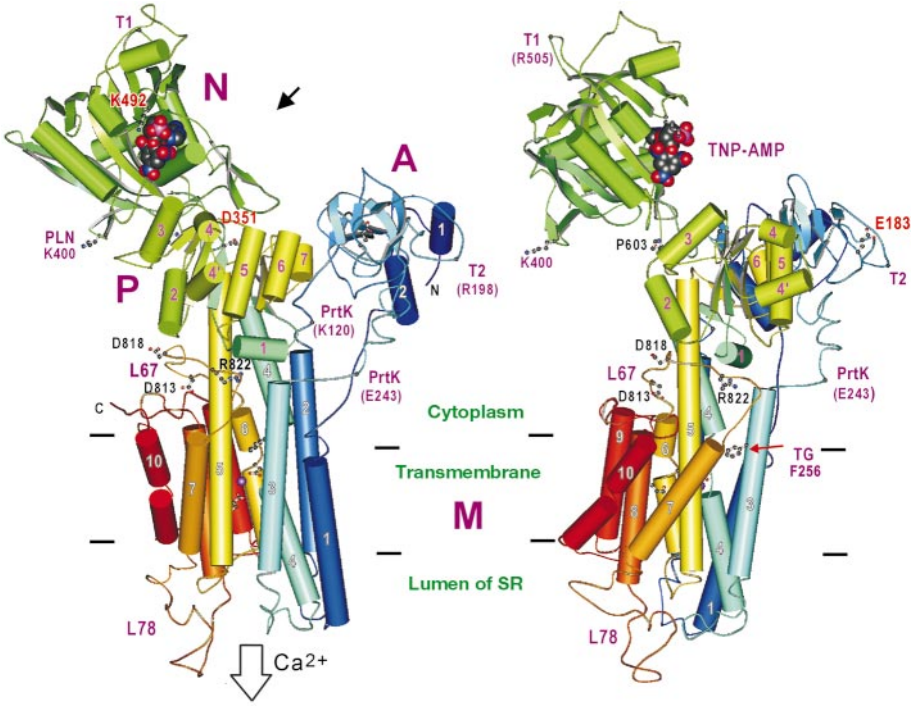

Figure 2 Architecture of the sarcoplasmic reticulum Ca^{2+}-ATPase. α-Helices are represented by cylinders and β-strands by arrows, as recognized by DSSP[46]. Cylinders are not used for one-turn helices. Colour changes gradually from the N terminus (blue) to the C terminus (red). Three cytoplasmic domains are labelled (A, N and P). Transmembrane helices (M1–M10) and those in domains A and P are numbered. The model is orientated so that transmembrane helix M5 is parallel to the plane of the paper. The model in the right panel is rotated by 50° around M5. The M5 helix is 60 Å long and serves as a scale. Several key residues are shown in ball-and-stick, and TNP-AMP by CPK. D351 is the residue of phosphorylation. Two purple spheres represent Ca^{2+} in the transmembrane binding sites. The binding sites for phospholamban (PLN)[16] and thapsigargin (TG)[17] are marked, as are major digestion sites for trypsin[5] (T1 and T2) and proteinase K[28] (PrtK). The arrow specifies the direction of view in Fig. 6b. Figure prepared with MOLSCRIPT[47].

Structure determination

The crystals were grown at pH 6.1 in the presence of 10 mM $CaCl_2$ and exogenous lipid. Electron microscopy of these crystals showed that the protein molecules were indeed embedded in lipid bilayers (data not shown). They were very thin (typically < 20 μm); but each of them allowed a full data set to be collected at SPring-8. The structure was solved by standard multiple isomorphous replacement (MIRAS) methods and refined to 2.6 Å resolution. The quality of the diffraction data and the refinement statistics are given in Table 1. The atomic model included about 250 water molecules in the cytoplasmic and the lumenal regions and about 30 in the transmembrane region. The distribution of hydration water molecules indicated approximately the position of the membrane boundary, which was roughly parallel to the *a* axis (Fig. 1).

Architecture of the sarcoplasmic reticulum Ca^{2+}-ATPase

The overall architecture of the sarcoplasmic reticulum Ca^{2+}-ATPase with bound Ca^{2+} is shown in Fig. 2. All 994 amino acid residues[15] were identified in the electron-density maps (see Fig. 3a, b for the initial maps). The molecule fits in a box of 100 Å × 80 Å × 140 Å. The cytoplasmic headpiece has a split appearance consisting of three well separated domains (designated as A, N and P). The phosphorylation site, Asp 351, is located in domain P, and, as described below, the adenosine moiety of nucleotide (here we used 2′,3′-*O*-(2,4,6-trinitrophenyl)-AMP (TNP-AMP)) is bound to domain N.

The transmembrane region (M) comprises ten α-helices (M1–M10), the arrangement of which is shown in Fig. 3a. There is a clear segregation between M1–M6 and M7–M10, consistent with the lack of M7–M10 helices in bacterial type I P-type ATPases (for example, ref. 2). The lengths of helices and the inclination to the membrane vary substantially (Fig. 2). Some of them (M2 and M5) are very long (~60 Å) and fairly straight, but some are unwound (M4 and M6) or kinked (M10) at the middle of the membrane. The helices that have been presumed to form Ca^{2+}-binding sites (M4–6, M8) show very different folding patterns, although similarity among them was expected from mutation studies[3]. M5 is located in the centre of the molecule and extends from the lumenal surface of the membrane to the centre of the cytosolic domain P, looking like the 'centre mast' of the enzyme. M2 and M3 are long helices that are rather isolated. The implication of this feature is discussed below. These long helices are continuous across the membrane surface and therefore treated as single helices, including the region previously assigned to 'stalk helices'[5]. Lumenal loops are short except for the one connecting M7 and M8 (L78, ~35 residues). In

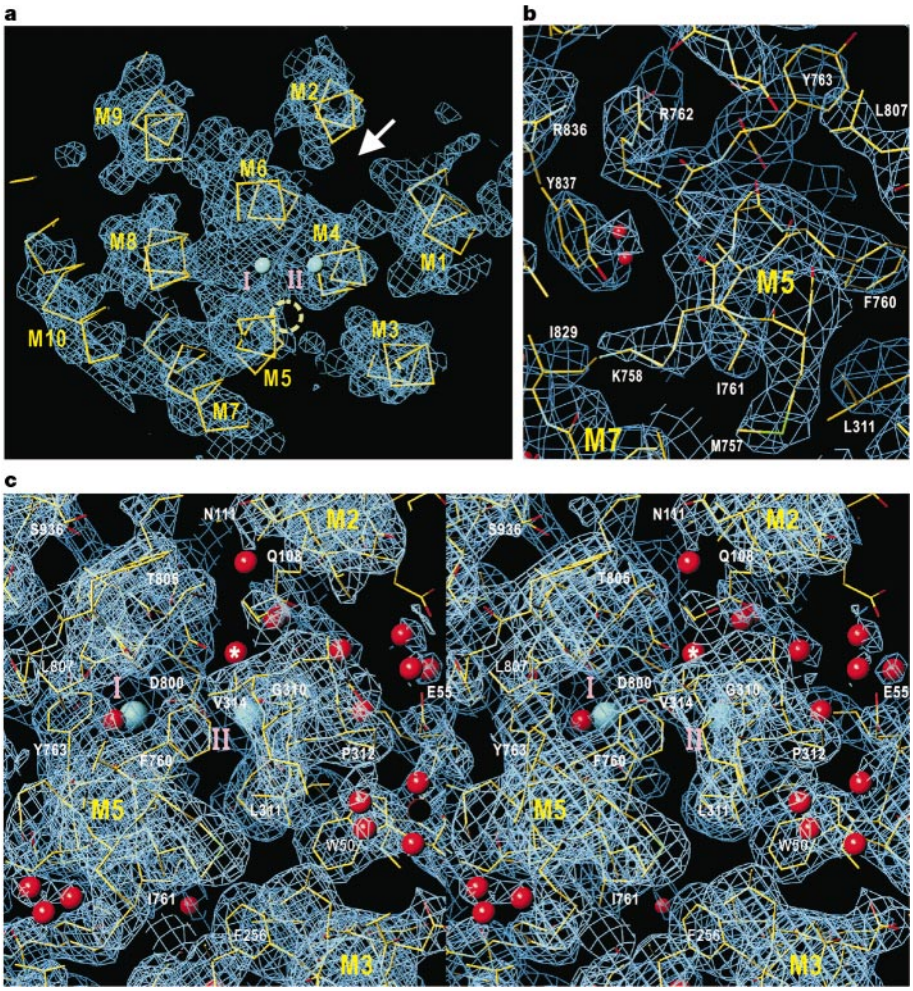

Figure 3 The arrangement of transmembrane helices (**a**), an enlarged view of a part of M5 helix (**b**) and water accessible cavities on the cytoplasmic surface (in stereo, **c**). The viewing direction is roughly normal to the membrane from the cytoplasmic side with domain A on the right hand side (**a**,**c**). The lumenal half including the Ca^{2+}-binding sites is shown in **a** and the cytoplasmic half in **c**. Cyan spheres represent two Ca^{2+} ions (I and II) and red spheres represent water molecules. A solvent flattened map is used in **a** and **b** (calculated at 2.8 Å resolution and contoured at 1.2σ), and a $2|F_o| - |F_c|$ composite omit map prepared with CNS[45] (calculated at 2.6 Å resolution and contoured at 1.5σ) in **c**. The arrow in **a** indicates the viewing direction in Fig. 4b. Circle in **a** indicates a likely position of the outlet of Ca^{2+} pathway. The water molecule found nearest to the Ca^{2+}-binding sites is marked (asterisk in **c**). Note that only M2, M3 and M5 are labelled in **c**.

Fig. 2, the major sites for protease digestion and the binding sites of phospholamban[16] and thapsigargin[17] are also identified.

Structure of the Ca^{2+}-binding sites

The M4–M6 and M8 helices surround two high-density peaks (Fig. 4), which we identify as two bound Ca^{2+} ions and not water. Our reasons are fourfold. (1) The level of density is too high to be explained by water—the temperature factor was refined to unreasonably low values (<2 Å^2) when water molecules were assigned but was appropriate when Ca^{2+} were assigned (~40 Å^2, similar to those of coordinating atoms). (2) At least six coordinating oxygen atoms are located at a distance of 2.2–2.6 Å from the centre of each site; this is unusual for a water molecule. (3) The valence values calculated from the geometry of coordinating atoms are 1.95 (I) and 2.15 (II), which qualify as high-affinity Ca^{2+}-binding sites[18]. (4) Omit difference maps showed the presence of a much smaller peak 2.4 Å away from the main one (Fig. 4, I). This peak had a density appropriate to a water molecule, as judged by the refined temperature factor.

These two sites are at similar heights with respect to the membrane (Fig. 1) and are 5.7 Å apart (Fig. 4). Following previous proposals, they are termed as sites I and II[3]. Site I is located in the space between the M5 and M6 helices with contribution from M8 at a rather distal position. The side-chain oxygen atoms of Asn 768, Glu 771 (M5), Thr 799, Asp 800 (M6) and Glu 908 (M8) contribute to this site, in agreement with mutational studies[6]. Disruption of helix conformation around Asp 800 and Gly 801 allows both Thr 799 and Asp 800 on M6 to contribute. All of the side-chain oxygen atoms, except for that of Glu 771, are arranged on roughly the same plane; that of Glu 771 coordinates from underneath (that is, the lumenal side of) the plane (Fig. 4b). In contrast, site II is formed almost 'on' helix M4 (Fig. 3a) by the main-chain carbonyl oxygen atoms of Val 304, Ala 305 and Ile 307 (M4) and the side-chain oxygen atoms of Asn 796, Asp 800 (M6) and Glu 309 (M4). Obviously, this kind of coordination geometry is only possible because helix M4 is unwound between Ile 307 and Gly 310. The PEGL motif in this unwound region has been recognized as a key motif[2]; the glutamate residue is replaced by cysteine or histidine in ATPases that transport heavy metals[2].

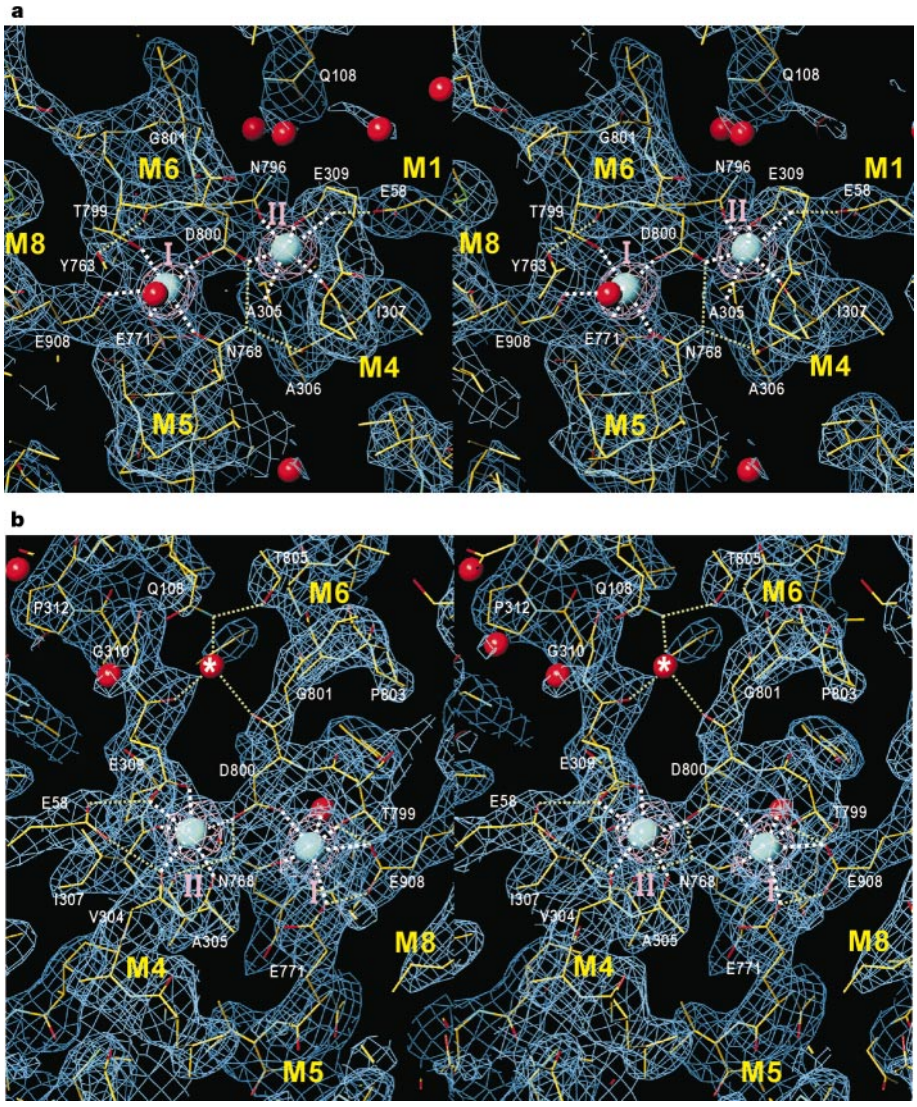

Figure 4 Details of the transmembrane Ca^{2+}-binding sites. The refined model is superimposed with a $2|F_o| - |F_c|$ composite-omit map prepared with CNS (blue meshes, contoured at 1.5σ). The meshes in pink show omit $|F_o| - |F_c|$ map for Ca^{2+} and a bound water (cut-off at 3σ). Blue spheres represent Ca^{2+}, and red spheres water molecules. Viewed roughly normal to the membrane from the cytoplasmic side (**a**) and parallel to the membrane (**b**) in stereo. The coordinations of oxygen atoms to Ca^{2+} are indicated by white dotted lines, and possible hydrogen bonds stabilizing the coordination geometry by green dashed lines. The viewing direction in **b** is also specified in Fig. 3a. Water molecule nearest to the Ca^{2+}-binding site is marked (asterisk). Note the unwinding of helices M4 and M6 and rows of exposed carbonyl oxygen atoms along these helices in **b**.

These two sites are stabilized by hydrogen-bond networks between the coordinating residues (for example, between Ala 306 and Asn 768) and between residues on other helices (for example, between Val 304 and Glu 309 on M4 and Glu 58 on M1, see Fig. 4). These hydrogen-bond networks must be important for the cooperative binding of two Ca^{2+} ions (ref. 19). As Asp 800 is coordinated to both Ca^{2+} atoms, the correct positioning of this residue must be very important. Furthermore, this residue is located in the unwound region between two helices (that is, the lumenal and cytoplasmic halves of M6) and the carbonyl oxygen atom is highly exposed (Fig. 4b), implying that the position of this key residue is under the control of other residues. This unwound conformation agrees well with an NMR study of isolated M6 polypeptide in detergent micelle[20].

An important question is: how do Ca^{2+} ions reach the transmembrane binding sites? Owing to the lack of large vestibules similar to those found in ion channels[21], our structure does not provide a definite answer. One candidate for Ca^{2+} entry is the area surrounded by M2, M4 and M6 (Fig. 3c). It is a cavity with a rather wide opening and is clearly water accessible (seven water molecules are seen in Fig. 3c). In the upper part of this cavity are located Gln 108 and Asn 111, a critical residue for ATPase activity[22]. Particularly interesting are the rows of exposed oxygen atoms formed by the unwound part of M4 (Pro 312 to Glu 309) and of M6 (Gly 801 and Asp 800). These rows of main-chain carbonyl oxygen atoms point towards the cytoplasm (Fig. 4b), providing a hydrophilic pathway leading to the Ca^{2+}-binding sites. The rows constrict near the Ca^{2+}-binding sites, trapping a water molecule (Figs 3c and 4b, asterisk); here, the oxygen atoms are arranged so that nearly ideal hydrogen-bonding geometry is provided for this water molecule. Such a geometry must be required for displacing water molecules[21] that are bound to Ca^{2+} much more tightly than to monovalent cations. The outlet of Ca^{2+} is likely to be located in the area surrounded by M3–M5 (Fig. 3a, circle); here too, a ring of oxygen atoms with bound water molecules is formed.

Thus, the unwinding of transmembrane helices appears to be required for two purposes: first, to realize efficient coordination geometry; and second, to provide rows of oxygen atoms for guiding Ca^{2+} to the binding site and removing water molecules at the same time.

Function and structure of three cytoplasmic domains

As described above, the cytoplasmic headpiece consists of three well separated domains. The central part is occupied by domain P, which contains the residue of phosphorylation (Asp 351). This domain is composed of two parts widely separated in the amino-acid sequence. The N-terminal part (roughly between Asn 330 and Asn 359) is connected to M4 and the C-terminal part (roughly Lys 605 to Asp 737) to M5. These two parts are assembled into a seven-stranded parallel β-sheet with eight short associated helices, together forming a typical Rossman fold (Fig. 5a). The residue of phosphorylation, Asp 351, is situated in the C-terminal end of the central β-strand (Fig. 5a), as is usually the case with nucleotide-binding proteins with a Rossman fold. Around this, the residues critical for ATP hydrolysis are clustered (Fig. 5a; see refs 2 and 4 for reviews) and form a highly negatively charged surface that is accessible to solvent (Fig. 6b).

In our structure, the folding pattern and the locations of the critical amino acids are essentially identical to those of the core domain of L-2-haloacid dehalogenase[23] (HAD; Fig. 5b), as predicted by sequence homology[8]. Using this homology, we can propose roles to some extent for the critical amino acids.

Domain N is the largest of the three cytoplasmic domains and has $M_r \approx 27$K. This domain is formed by the residues inserted (roughly Gln 360–Arg 604) between the two regions constituting domain P and corresponds to the sub-domain in HAD. It comprises a seven-stranded antiparallel β-sheet with two helix bundles sandwiching it (Fig. 2; see also Fig. 7b for a top view). A function of this domain became clear when we directly visualized bound nucleotide. To do this, we soaked the crystals in 0.5 mM TNP-AMP solution and identified the nucleotide's position by difference Fourier methods (Table 1). In the difference Fourier map (Fig. 6a), TNP-AMP is located unambiguously near Phe 487, which has been identified as a critical residue for ATP binding[24]. Well characterized residues such as Lys 515 and Lys 492 are located nearby (Fig. 6a). Lys 515, thought for a long time to be at the 'mouth' of the ATP-binding pocket[25], is actually located in the depth of the binding pocket (Fig. 6b). The close proximity of Lys 515 to the adenosine moiety (~5Å, Fig. 6a) explains the inhibition of high-affinity ATP binding by chemical modification of this residue with fluorescein isothiocyanate[25]. Lys 492, labelled with 8-azido-TNP-AMP/ATP[26]

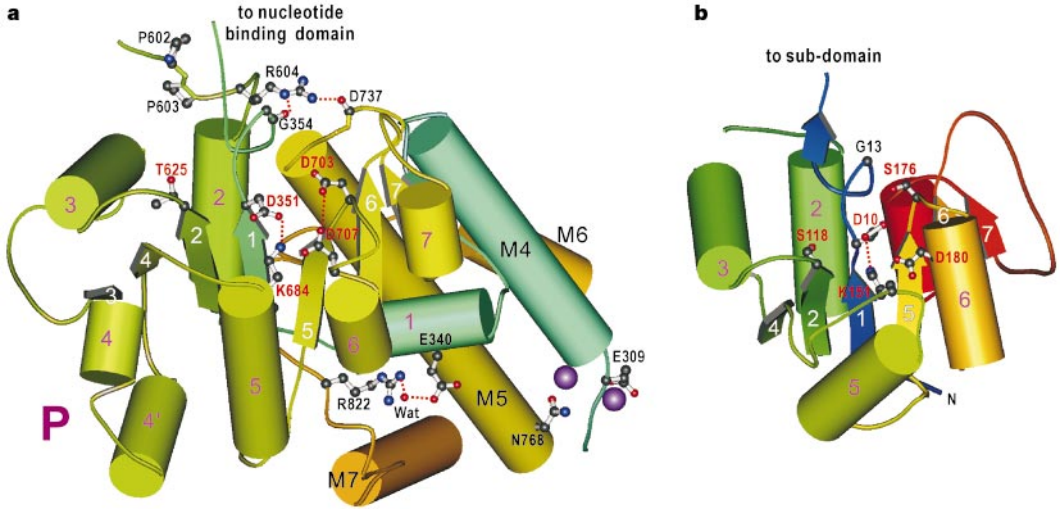

Figure 5 Architecture of the phosphorylation domain (P in Fig. 2) of Ca^{2+}-ATPase (**a**) and the catalytic core domain of L-2-haloacid dehalogenase (HAD[23], **b**). Critical amino-acid residues found in HAD are all preserved and indicated in **a**. D351 is the phosphorylation site in Ca^{2+}-ATPase (**a**), corresponding to D10 in HAD (**b**). Three residues (Thr 625 to Asp 627) forming the loop connecting β-strand 2 and α-helix 3 are all critical for ATPase activity[48]. Lys 684 is labelled by ATP pyridoxal[27] and Asp 703 and Asp 707 are labelled by ClRATP with Na^+K^+-ATPase[49]. Colour coding is as in Fig. 2. Numbering of the secondary structures in **b** is made consistent with **a** and different from the original[23]. Red dashed lines show possible hydrogen bonds. Figure prepared with MOLSCRIPT[47].

and other ATP-derivatives[27] is located in a short loop connecting the β-strands (Lys 492 is marked in Fig. 2; also see Fig. 7b for a top view). This binding pocket is positively charged, in marked contrast to the region around the phosphorylation site (Fig. 6b).

Domain A is the smallest of the three domains and has $M_r \approx 16K$. It comprises roughly the 110 residues between M2 and M3 (previously called the transduction domain[5] or β-strand domain), which form a distorted jelly roll structure, and the 40 residues of the N-terminal part of the enzyme, which form two short helices. This domain is connected to the transmembrane region by long loops and is nearly isolated. The susceptibility of the loops to proteinase K attack is affected by Ca^{2+} (ref. 28). The well conserved TGES motif (starting at Thr 181) is located at an edge of this domain (E183 is shown in Fig. 2). Arg 198, trypsin digestion at which is enhanced by Ca^{2+} and blocked by phosphorylation[29], is located at the outermost loop (T2 in Fig. 2). All these biochemical data suggest that this domain moves substantially during active transport.

Expected structure in the absence of Ca^{2+}

As mentioned above, the cytoplasmic headpiece has a compact appearance in the maps derived from tubular crystals[12,13]. The most likely reason for this difference from the present structure is the crystallization conditions: the tubular crystals are formed in the absence of Ca^{2+} and in the presence of decavanadate, whereas our three-dimensional crystals are formed in the presence of 10 mM Ca^{2+}. To examine whether the difference could be explained by domain motions, we fitted the atomic model to a low-resolution map (8 Å) from tubular crystals[13]. This was done first by cutting out the cytoplasmic domains (A, N and P) and then by searching for the best matching positions individually (Fig. 7). The ridges of all surface helices match the density map (blue net) very well. Furthermore, a high-density peak (small sphere in Fig. 7), probably a vanadate oligomer, is found in close proximity to Asp 351. Closer examination shows that a few hydrogen bonds can be readily made at the domain interface.

The fitting of these three cytoplasmic domains leaves one spherical lobe of high density (Fig. 7a, large sphere) unidentified. Its density and size indicate that it is probably decavanadate ($V_{10}O_{28}^{6-}$). This lobe is located at the side of the highly positively charged groove formed by domains N and P (Fig. 6b). The groove is narrower than in the present structure (by ~20°) and decavanadate fits in the lobe (Fig. 7a), like a ball in jaws preventing the jaws from closing. Arg 489, Lys 492 (in the red loop in domain N in Fig. 7) and Arg 678 (see Fig. 6b) are expected to participate in the binding of this large anion. This location of decavanadate will explain its inhibitory effect on ATPase activity.

To realize this arrangement, all the cytoplasmic domains have to move with respect to the M4 and M5 helices, which do not fit the density map in Fig. 7 and need to be inclined by ~20°. Domain A undergoes the largest movement of the three (nearly a 90° rotation). The TGES loop starting at Thr 181 (Fig. 7, red loop in domain A) meets the TGD motif starting at Thr 625 (Fig. 7, red loop in domain P; see also Fig. 5a). The critical importance of these two motifs has been well documented[2]. The counterpart of Thr 625 in HAD is Ser 118 (Fig. 5b), which is thought to be the binding residue of the substrate carboxyl group[30]. The gathering of these loops in the E2 or E2P state has been demonstrated with Na^+K^+-ATPase[31].

The large movement of domain A requires changes in the orientations of the M1–M3 helices, consistent with the changes in sensitivity to proteases as mentioned previously[28]. Domain N has changed its orientation by ~20° with respect to domain P, resulting in a similar orientation—when projected along the *b* axis—to that observed with three-dimensional microcrystals by electron microscopy[14]. Despite the poor agreement of helices M4 and M5, the loop connecting helices M6 and M7 (L67) fits well with the density map (Fig. 7a), indicating that it follows domain P. But its position with respect to the membrane helices is different, being much higher above the membrane surface than in the presence of Ca^{2+}. This feature suggests that L67 is important for concerted domain motions.

Role of the loop connecting helices M6 and M7

This loop (L67) runs along the bottom of domain P and in a position that can mediate interactions of domain P and the transmembrane domain (Fig. 8). The P2 helix will link the movements of M5 and the DPPR region, and the P1 helix will couple those of M4 and the central β-strand on which Asp 351 is located (also see Fig. 5a). Thus, this loop interacts directly or indirectly with most of the key parts of the enzyme. If domain P moves or the upper

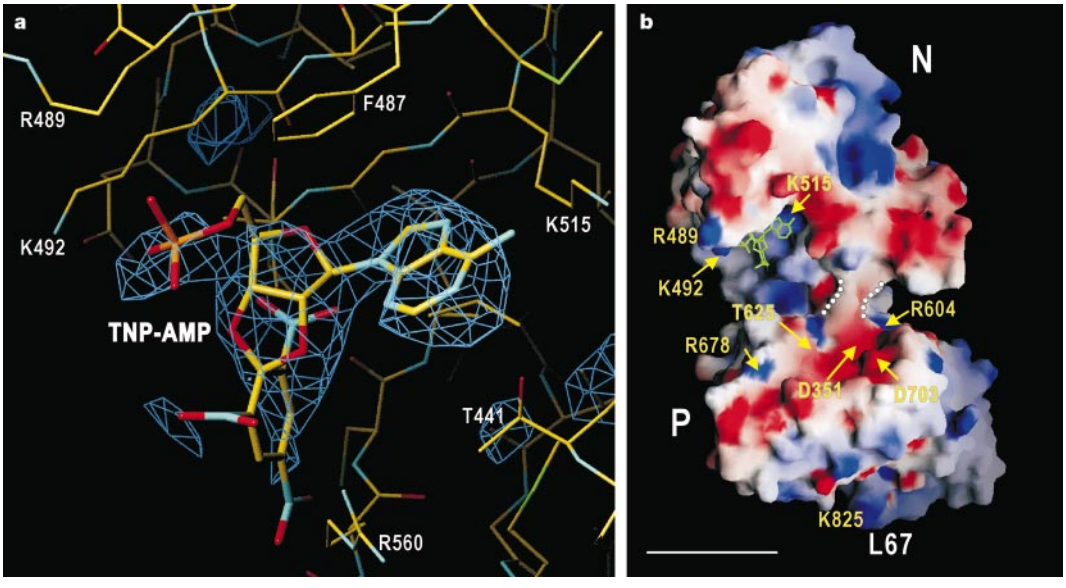

Figure 6 Binding of TNP-AMP to Ca^{2+}-ATPase. Difference Fourier map showing the electron density of bound TNP-AMP (**a**) and a surface potential map (red, negatively charged; blue, positively charged) of domains N and P prepared with Grasp[50] (**b**). The final model of the protein part (refined without TNP-AMP) and a rough model of TNP-AMP are superimposed (**a**). The map was calculated at 4.0 Å resolution and contoured at 2.5σ (**a**). In **b**, a stick model of TNP-AMP is placed in the position defined in **a**. White circles identify the bridging region between domains N and P. Note that the distances between the TNP-AMP and the phosphorylation site (D351), and between K492 and R684, which are crosslinked by glutaraldehyde, are more than 25 Å. The direction of view in **b** is indicated in Fig. 2. Scale bar, 20 Å.

part of helix M5 or M4 moves, as suggested by the comparison with the map from tubular crystals, the movement will be transmitted to M3 and M6. Because L67 is directly connected to M6, changes induced in M6 by the binding of Ca^{2+} will be transmitted to domain P through L67 and the P1 or P2 helix.

The comparison with the map from tubular crystals also suggests a conformation change in L67. In this regard, the results of scanning cysteine mutagenesis are interesting. The pair of residues that formed disulphide bridges in the absence of Ca^{2+} were compatible with our atomic model for the lumenal half but not for the cytoplasmic half of helix M6[32]. These results indicate that the cytoplasmic half of M6 may undergo rotation or winding/unwinding during Ca^{2+} transport in concert with the movement of L67. In fact, the geometry of this region is far from an ideal helix and is not recognized as such, depending on the classification program.

Thus, it is likely that this loop is important in coordinating different parts of the enzyme. In this way it may affect Ca^{2+} binding and ATP hydrolysis[33]. Asp 813 and Asp 818 were postulated to be the initial Ca^{2+}-binding sites[33], but in this configuration they are separated by ~10 Å (Fig. 2) and are unable to form a Ca^{2+}-binding site.

Large domain motion during ATP-hydrolysis

The phosphorylation site (Asp 351) is more than 25 Å away from the bound nucleotide (Fig. 6b). This means that domain closure must occur during ATP hydrolysis. Also, the two residues crosslinked by glutaraldehyde (Lys 492 and Arg 678; ref. 34) are separated by more than 25 Å (Fig. 6b). ATP pyridoxal labels both Lys 492 and Lys 684 in the absence of Ca^{2+} but only Lys 684 (Fig. 5a) in the presence of Ca^{2+} (ref. 27). Fluorescence from TNP-AMP increases during the catalytic cycle and on phosphorylation by Pi (ref. 35). Phosphorescence spectroscopy (of erythrosin isothiocyanate attached to Lys 464 in domain N) showed large domain motions induced by the binding of Ca^{2+} (ref. 36). All these data indicate that domain N is mobile in the presence of Ca^{2+} but fixed in its absence, and that domain N comes close to domain P in the phosphorylated states by thermal fluctuation and/or by conformation changes induced by ATP-binding. Stabilization of the 'occluded' state by chromium-ATP[4] is likely to be a result of crosslinking of domains N and P by chromium-ATP.

Large domain motions require the presence of a hinge region. Domain N can be isolated by several proteases[37], suggesting that the region around Ser 350 and Gly 609 is indeed flexible. In fact, the connection between domains N and P appears to be extremely tenuous (Figs 2 and 6b), with a well conserved Gly 354 and the invariant DPPR motif[2] (Fig. 5a). Furthermore, the hydrogen-bond network involving Gly 354, Arg 604 and Asp 737 to Asn 739 seems to link the movement of this hinge region to that of M5, thereby effectively transmitting the phosphorylation signal to the Ca^{2+}-binding sites.

How does Ca^{2+} binding to the high-affinity sites induce large domain motions? It is tempting to postulate that domain A works as an actuator or an anchor for the movement of domain N. As already described, the susceptibility to proteases of the loops connecting domain A to the transmembrane helices changes depending on Ca^{2+} (refs 28, 29), consistent with the idea that Ca^{2+} binding releases domain A. This movement must be made by helices M1–M3, which have only a few hydrogen bonds with other parts of the enzyme. For example, M3 is hydrogen-bonded to L67 near the cytoplasmic end (Fig. 8) and only with M4 at either end. Exactly the same applies to M2. M1 has hydrogen bonds with M4 only, and the residues involved are Glu 309 (Fig. 4) and Lys 297, which are both critical residues[6]. Therefore, Ca^{2+} binding probably stabilizes these hydrogen bonds while destabilizing others, and moves M1–M3 to release domain A. In this regard, it is particularly interesting that thapsigargin, a very potent inhibitor[38], is supposed to bind to the region where M3, M4 and L67 gather (around Phe 256; ref. 17; Fig. 8). This must be a very strategic point for fixing them in one configuration. As already noted, L67 may work as a linker between different domains to elicit large-scale domain motions for transporting ions against a concentration gradient.

Conclusion

We have described the atomic model of Ca^{2+}-ATPase with bound

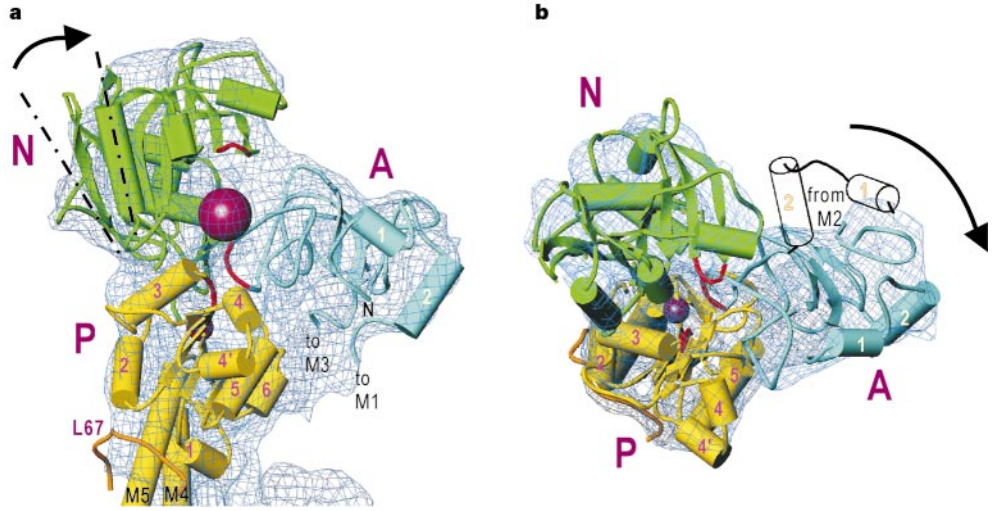

Figure 7 Fitting the atomic model obtained for the Ca^{2+}-bound state (arrows and cylinders) to an 8 Å resolution map (blue net) obtained from tubular crystals formed in the absence of Ca^{2+} and presence of decavanadate and dansyl-thapsigargin[13]. Fitting was done by rigid body motions of three cytoplasmic domains (A, N and P). Large sphere represents a decavanadate ion ($V_{10}O_{28}^{6-}$). Small sphere represents the high-density peak around Asp 351; in **a**, it is located between helices P3 and P4′. Red loops correspond to the TGES motif (starting at Thr 181) in domain A (cyan), the RDRK motif (starting at Arg 489) in domain N (green) and the TGD motif (starting at Thr 625) in domain P (yellow). Overall orientation of the molecule in **a** is the same as in Fig. 2a. In **b**, it is viewed from the cytoplasmic side normal to the membrane. Two dashed–dotted lines in **a** show the orientation of the longest helix in domain N to approximate the movement of domain N (the direction indicated by the arrow). Open cylinders are drawn in **b** for the same purpose (showing the positions of A1 and A2 helices when whole cytoplasmic domains moved as a rigid body to the best fitting position for domain P). The orientation of domain P with respect to M4 and M5 is different from that in 10 mM Ca^{2+}. Hence the fitting of M4 and M5 is poor but can be much improved by inclining them by ~20°. The residues included for fitting are 1–42 and 125–233 (A), 359–602 (N), and 330–357 and 605–740 (P).

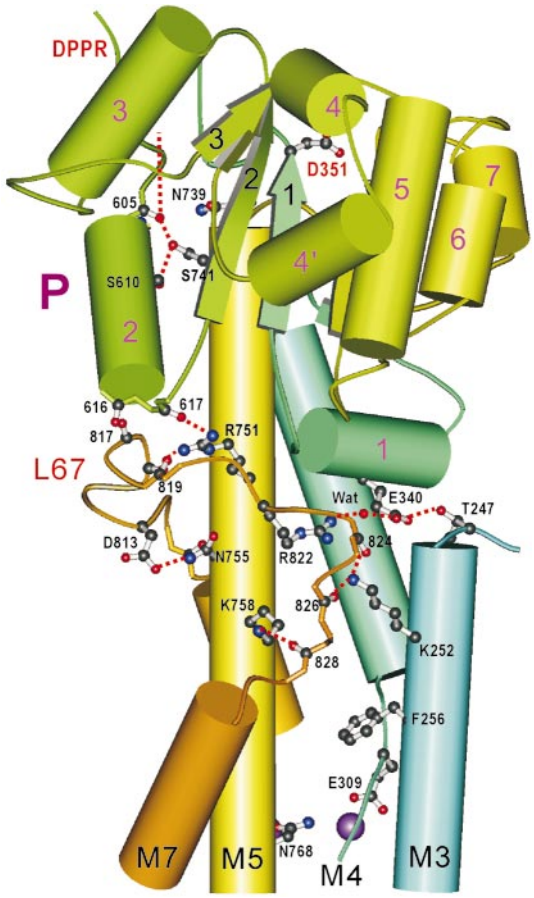

Figure 8 Coupling of the phosphorylation domain and the transmembrane domain by the loop (L67) connecting helices M6 and M7. L67 runs along the bottom of domain P and seems to be important in transmitting signal between the phosphorylation site and the Ca^{2+}-binding sites, which are separated by ~50 Å. As depicted, there are extensive hydrogen bonds (blue dotted lines) between this loop and various helices, as well as van der Waals contacts (not shown). Colour coding is as in Fig. 2. F256 is involved in thapsigargin binding[17].

Ca^{2+} on the basis of X-ray diffraction data at 2.6 Å resolution. Our model explains many more experimental results than we can describe here. We have shown that the cytoplasmic region consists of three well separated domains and have proposed new names for them: domain A may work as an actuator or an anchor for domain N, which binds nucleotides; and domain P contains Asp 351, the residue of phosphorylation. The finding that the binding site for the adenosine moiety and the phosphorylation site are located on different domains will settle much of the controversy on the ATP-binding site(s)[4]. We also have described how two Ca^{2+} ions are bound to their transmembrane binding sites and have proposed a possible pathway for Ca^{2+}. We have fitted the atomic model to a low-resolution map of the enzyme without Ca^{2+} but with decavanadate bound, and shown approximate configurations of different domains in this state. This comparison has indicated a mechanism for how the cytoplasmic domains communicate with the helices that form the Ca^{2+}-binding site, which is more than 50 Å away (the distance between the ATP-binding pocket and the bound Ca^{2+} ions is ~80 Å). □

Methods

Ca^{2+}-ATPase was prepared from rabbit hind leg muscle and purified using affinity column chromatography[11] after solubilization using octaethyleneglycol mono-*n*-dodecylether ($C_{12}E_8$). Crystals were grown by dialysing the mixture of purified protein and phospholipid (phosphatidylcholine) against crystallization buffer[39] containing 0.8 M sodium butyrate, 2.75 M glycerol, 10 mM $CaCl_2$, 3 mM $MgCl_2$, 2.5 mM NaN_3, 0.2 mM dithiothreitol and 20 mM MES, pH 6.1. After one month of incubation, the crystals were grown to typically 100 × 500 × <20 μm. The crystals belonged to space group *C*2 with unit cell parameters of $a = 166.0$ Å, $b = 64.4$ Å, $c = 147.1$ Å, $\beta = 98.0°$ (at 100 K), and contained one protein molecule in the asymmetric unit. The thickness of the crystals used for diffraction experiments was occasionally measured by freeze-substitution and sectioning of the crystals. The crystals were picked up using nylon loops and flash-frozen in cold nitrogen gas from a cryostat (Rigaku). Heavy-atom derivatives were prepared by soaking for 1 h. Phase information of the (h k 0) plane derived from electron micrographs of the thinner crystals was very useful in efficient screening of derivatives with a laboratory X-ray source. Final data were all collected at SPring-8 (beam lines BL41XU (ref. 40) and BL44B2 (ref. 41)) using either Rigaku R-AXIS IV or Mar CCD 165 detectors.

Data taken with R-AXIS IV were processed with Denzo and Scalepack[42] and those with the CCD detectors were processed with MOSFLM[43] and Scala[44]. Merging of different data sets for native data was done using Scalepack. Subsequent data processing was carried out using CCP4 program suites[44]. Experimental phases were first calculated by Mlphare[44] to 2.8 Å resolution derived from five platinum and three lanthanide derivatives (Table 1). The mean figure of merit for acentric reflections was 0.558 (20.0–2.8 Å) and 0.294 in the last resolution shell (3.17–2.80 Å). The map refined by density modification with Solomon[44] (Fig. 3a, b) was used for the initial modelling with Turbo-Frodo (BioGraphics). For structure refinement CNS[45] was used. The refined temperature factors were 60.0 $Å^2$ for protein atoms, 48.7 $Å^2$ for bound water molecules and 41.3 $Å^2$ for Ca^{2+}. The assignment of secondary structures was done using the program DSSP[46]. Fitting of the atomic model to the low resolution map by electron microscopy was first done manually using Turbo-Frodo and then refined by calculating the correlation function with magnification correction of the electron microscopy map.

Received 9 March; accepted 4 May 2000.

1. Ebashi, S. & Lipman, F. Adenosine triphosphate-linked concentration of calcium ions in a particulate fraction of rabbit muscle. *J. Cell. Biol.* **14,** 389–400 (1962).
2. Møller, J. V., Juul, B. & le Maire, M. Structural organization, ion transport, and energy transduction of P- type ATPases. *Biochim. Biophys. Acta* **1286,** 1–51 (1996).
3. MacLennan, D. H., Rice, W. J. & Green, N. M. The mechanism of Ca^{2+} transport by sarco(endo)-plasmic reticulum Ca^{2+}-ATPases. *J. Biol. Chem.* **272,** 28815–28818 (1997).
4. McIntosh, D. B. The ATP binding sites of P-type ion transport ATPases. *Adv. Mol. Cell. Biol.* **23A,** 33–99 (1998).
5. MacLennan, D. H., Brandl, C. J., Korczak, B. & Green, N. M. Amino-acid sequence of a Ca^{2+} + Mg^{2+}-dependent ATPase from rabbit muscle sarcoplasmic reticulum, deduced from its complementary DNA sequence. *Nature* **316,** 696–700 (1985).
6. Clarke, D. M., Loo, T. W., Inesi, G. & MacLennan, D. H. Location of high affinity Ca^{2+}-binding sites within the predicted transmembrane domain of the sarcoplasmic reticulum Ca^{2+}- ATPase. *Nature* **339,** 476–478 (1989).
7. Saraste, M., Sibbald, P. R. & Wittinghofer, A. The P-loop—a common motif in ATP- and GTP-binding proteins. *Trends Biochem. Sci.* **15,** 430–434 (1990).
8. Aravind, L., Galperin, M. Y. & Koonin, E. V. The catalytic domain of the P-type ATPase has the haloacid dehalogenase fold. *Trends Biochem. Sci.* **23,** 127–129 (1998).
9. Dux, L. & Martonosi, A. Two-dimensional arrays of proteins in sarcoplasmic reticulum and purified Ca^{2+}-ATPase vesicles treated with vanadate. *J. Biol. Chem.* **258,** 2599–2603 (1983).
10. Dux, L., Pikula, S., Mullner, N. & Martonosi, A. Crystallization of Ca^{2+}-ATPase in detergent-solubilized sarcoplasmic reticulum. *J. Biol. Chem.* **262,** 6439–6442 (1987).
11. Stokes, D. L. & Green, N. M. Three-dimensional crystals of CaATPase from sarcoplasmic reticulum. Symmetry and molecular packing. *Biophys. J.* **57,** 1–14 (1990).
12. Toyoshima, C., Sasabe, H. & Stokes, D. L. Three-dimensional cryo-electron microscopy of the calcium ion pump in the sarcoplasmic reticulum membrane. *Nature* **362,** 467–471 (1993).
13. Zhang, P., Toyoshima, C., Yonekura, K., Green, N. M. & Stokes, D. L. Structure of the calcium pump from sarcoplasmic reticulum at 8-Å resolution. *Nature* **392,** 835–839 (1998).
14. Ogawa, H., Stokes, D. L., Sasabe, H. & Toyoshima, C. Structure of the Ca^{2+} pump of sarcoplasmic reticulum: a view along the lipid bilayer at 9-Å resolution. *Biophys. J.* **75,** 41–52 (1998).
15. Brandl, C. J., deLeon, S., Martin, D. R. & MacLennan, D. H. Adult forms of the Ca^{2+}ATPase of sarcoplasmic reticulum. Expression in developing skeletal muscle. *J. Biol. Chem.* **262,** 3768–3774 (1987).
16. Toyofuku, T., Kurzydlowski, K., Tada, M. & MacLennan, D. H. Amino acids Lys-Asp-Asp-Lys-Pro-Val^{402} in the Ca^{2+}-ATPase of cardiac sarcoplasmic reticulum are critical for functional association with phospholamban. *J. Biol. Chem.* **269,** 22929–22932 (1994).
17. Yu, M. *et al.* Specific substitutions at amino acid 256 of the sarcoplasmic/endoplasmic reticulum Ca^{2+} transport ATPase mediate resistance to thapsigargin in thapsigargin-resistant hamster cells. *J. Biol. Chem.* **273,** 3542–3546 (1998).
18. Nayal, M. & Di Cera, E. Predicting Ca^{2+}-binding sites in proteins. *Proc. Natl Acad. Sci. USA* **91,** 817–821 (1994).
19. Inesi, G., Kurzmack, M., Coan, C. & Lewis, D. E. Cooperative calcium binding and ATPase activation in sarcoplasmic reticulum vesicles. *J. Biol. Chem.* **255,** 3025–3031 (1980).
20. Soulié, S. *et al.* NMR conformational study of the sixth transmembrane segment of sarcoplasmic reticulum Ca^{2+}-ATPase. *Biochemistry* **38,** 5813–5821 (1999).
21. Doyle, D. A. *et al.* The structure of the potassium channel: molecular basis of K^+ conduction and selectivity. *Science* **280,** 69–77 (1998).
22. Clarke, D. M. *et al.* Functional consequences of glutamate, aspartate, glutamine, and asparagine mutations in the stalk sector of the Ca^{2+}-ATPase of sarcoplasmic reticulum. *J. Biol. Chem.* **264,** 11246–11251 (1989).
23. Hisano, T. *et al.* Crystal structure of L-2-haloacid dehalogenase from *Pseudomonas* sp. YL. An α/β hydrolase structure that is different from the α/β hydrolase fold. *J. Biol. Chem.* **271,** 20322–20330 (1996).
24. McIntosh, D. B., Woolley, D. G., Vilsen, B. & Andersen, J. P. Mutagenesis of segment ^{487}Phe-Ser-Arg-Asp-Arg-Lys^{492} of sarcoplasmic reticulum Ca^{2+}-ATPase produces pumps defective in ATP binding. *J. Biol. Chem.* **271,** 25778–25789 (1996).
25. Pick, U. Interaction of fluorescein isothiocyanate with nucleotide-binding sites of the Ca-ATPase from sarcoplasmic reticulum. *Eur. J. Biochem.* **121,** 187–195 (1981).

26. McIntosh, D. B., Woolley, D. G. & Berman, M. C. 2′,3′-*O*-(2,4,6-trinitrophenyl)-8-azido-AMP and-ATP photolabel Lys-492 at the active site of sarcoplasmic reticulum Ca^{2+}-ATPase. *J. Biol. Chem.* **267,** 5301–5309 (1992).
27. Yamamoto, H., Imamura, Y., Tagaya, M., Fukui, T. & Kawakita, M. Ca^{2+}-dependent conformational change of the ATP-binding site of Ca^{2+}-transporting ATPase of sarcoplasmic reticulum as revealed by an alteration of the target-site specificity of adenosine triphosphopyridoxal. *J. Biochem. (Tokyo)* **106,** 1121–1125 (1989).
28. Juul, B. *et al.* Do transmembrane segments in proteolyzed sarcoplasmic reticulum Ca^{2+}- ATPase retain their functional Ca^{2+} binding properties after removal of cytoplasmic fragments by proteinase K? *J. Biol. Chem.* **270,** 20123–20134 (1995).
29. Andersen, J. P., Vilsen, B., Collins, J. H. & Jørgensen, P. L. Localization of E1–E2 conformational transitions of sarcoplasmic reticulum Ca-ATPase by tryptic cleavage and hydrophobic labeling. *J. Membr. Biol.* **93,** 85–92 (1986).
30. Li, Y. F. *et al.* Crystal structures of reaction intermediates of L-2-haloacid dehalogenase and implications for the reaction mechanism. *J. Biol. Chem.* **273,** 15035–15044 (1998).
31. Goldshleger, R. & Karlish, S. J. D. Fe-catalyzed cleavage of the alpha subunit of Na/K-ATPase: evidence for conformation-sensitive interactions between cytoplasmic domains. *Proc. Natl Acad. Sci. USA* **94,** 9596-9601 (1997).
32. Rice, W. J., Green, N. M. & MacLennan, D. H. Site-directed disulfide mapping of helices M4 and M6 in the Ca^{2+} binding domain of SERCA1a, the Ca^{2+} ATPase of fast twitch skeletal muscle sarcoplasmic reticulum. *J. Biol. Chem.* **272,** 31412–31419 (1997).
33. Falson, P. *et al.* The cytoplasmic loop between putative transmembrane segments 6 and 7 in sarcoplasmic reticulum Ca^{2+}-ATPase binds Ca^{2+} and is functionally important. *J. Biol. Chem.* **272,** 17258–17262 (1997).
34. McIntosh, D. B. Glutaraldehyde cross-links Lys-492 and Arg-678 at the active site of sarcoplasmic reticulum Ca^{2+}-ATPase. *J. Biol. Chem.* **267,** 22328–22335 (1992).
35. Nakamoto, R. K. & Inesi, G. Studies of the interactions of 2′,3′-*O*-(2,4,6- trinitrocyclohexyldienylidine)adenosine nucleotides with the sarcoplasmic reticulum (Ca^{2+} + Mg^{2+})-ATPase active site. *J. Biol. Chem.* **259,** 2961–2970 (1984).
36. Huang, S. & Squier, T. C. Enhanced rotational dynamics of the phosphorylation domain of the Ca-ATPase upon calcium activation. *Biochemistry* **37,** 18064–18073 (1998).
37. Champeil, P. *et al.* Characterization of a protease-resistant domain of the cytosolic portion of sarcoplasmic reticulum Ca^{2+}-ATPase. *J. Biol. Chem.* **273,** 6619–6631 (1998).
38. Sagara, Y. & Inesi, G. Inhibition of the sarcoplasmic reticulum Ca^{2+} transport ATPase by thapsigargin at subnanomolar concentrations. *J. Biol. Chem.* **266,** 13503–13506 (1991).
39. Misra, M., Taylor, D., Oliver, T. & Taylor, K. Effect of organic anions on the crystallization of the Ca^{2+}-ATPase of muscle sarcoplasmic reticulum. *Biochim. Biophys. Acta* **1077,** 107–118 (1991).
40. Kamiya, N. *et al.* Design of the high energy undulator pilot beamline for macromolecular crystallography at the SPring-8. *Rev. Sci. Instrum.* **66,** 1703–1705 (1995).
41. Adachi, S., Oguchi, T. & Ueki, T. Present status of RIKEN beamline II (BL44B2) for structural biology. *SPring-8 Annual Report* **1,** 239–240 (1996).
42. Otwinowski, Z. & Minor, W. Processing of X-ray diffraction data collected in oscillation mode. *Methods Enzymol.* **276,** 307–325 (1997).
43. Leslie, A. G. W. MOSFLM- recent changes and future developments. *CCP4 Newsletter on Protein Crystallography* **35,** 18–19 (1998).
44. Collaborative Computational project, No. 4. The CCP4 suite: programs for protein crystallography. *Acta Crystallogr. D* **50,** 760–763 (1994).
45. Brünger, A. T. *et al.* Crystallography & NMR system: A new software suite for macromolecular structure determination. *Acta Crystallogr. D* **54,** 905–921 (1998).
46. Kabsch, W. & Sander, C. Dictionary of protein secondary structure: pattern recognition of hydrogen-bonded and geometrical features. *Biopolymers* **22,** 2577–2637 (1983).
47. Kraulis, P. J. MOLSCRIPT: a program to produce both detailed and schematic plots of protein structures. *J. Appl. Crystallogr.* **24,** 946–950 (1991).
48. Clarke, D. M., Loo, T. W. & MacLennan, D. H. Functional consequences of alterations to amino acids located in the nucleotide binding domain of the Ca^{2+}-ATPase of sarcoplasmic reticulum. *J. Biol. Chem.* **265,** 22223–22227 (1990).
49. Ovchinnikov, Y. *et al.* Affinity modification of E1-form of Na^+, K^+-ATPase revealed Asp-710 in the catalytic site. *FEBS Lett.* **217,** 111–116 (1987).
50. Nicholls, A., Sharp, K. A. & Honig, B. Protein folding and association: insights from the interfacial and thermodynamic properties of hydrocarbons. *Proteins Struct. Funct. Genet.* **11,** 281–296 (1991).

Acknowledgements

We thank S. Adachi, N. Kamiya (Riken) and M. Kawamoto (JASRI) for their help in data taking at SPring-8, and K. Tani for computations. We acknowledge that very first crystals for X-ray were made by H. Mukai. This work was supported in part by grants-in-aid from the Ministry of Culture, Education, Science and Sports of Japan and from CRESTO (to C.T. and M.N.) and also by Toray Science Foundation (C.T.). This paper is dedicated to S. Ebashi, a founder of Ca^{2+}-ATPase field and the father of the calcium theory.

Correspondence and requests for materials should be addressed to C.T. (e-mail: ct@iam.u-tokyo.ac.jp).

The atomic coordinates have been deposited in the PDB (accession code 1EUL).